R&D 5544-MS-01

(2)

AD

PARTICULATE CERAMIC MATRIX COMPOSITES FOR HIGH STRAIN-RATE PERFORMANCE

Final Technical Report

by

D.G.Brandon, Y.Yeshurun, L.Baum, M.Farkash and N.Shafry

August, 1990

United States Army

EUROPEAN RESEARCH OFFICE OF THE U.S.ARMY

London England

CONTRACT NUMBER DAJA45-88-C-0007

Technion - Israel Institute of Technology
Department of Materials Engineering
Haifa 32000, Israel

SECURITY CLASSIFICATION OF THIS PAGE

REPORT DOCUMENTATION PAGE

Form Approved
OMB No. 0704-0188

1a. REPORT SECURITY CLASSIFICATION	1b. RESTRICTIVE MARKINGS
2a. SECURITY CLASSIFICATION AUTHORITY	3. DISTRIBUTION/AVAILABILITY OF REPORT
2b. DECLASSIFICATION/DOWNGRADING SCHEDULE	
4. PERFORMING ORGANIZATION REPORT NUMBER(S) 040-0374	5. MONITORING ORGANIZATION REPORT NUMBER(S)
6a. NAME OF PERFORMING ORGANIZATION Technion R&D Foundation 6b. OFFICE SYMBOL (If applicable)	7a. NAME OF MONITORING ORGANIZATION
6c. ADDRESS (City, State, and ZIP Code) Technion City, Haifa 32000, Israel	7b. ADDRESS (City, State, and ZIP Code)
8a. NAME OF FUNDING/SPONSORING ORGANIZATION USACCE 8b. OFFICE SYMBOL (If applicable)	9. PROCUREMENT INSTRUMENT IDENTIFICATION NUMBER DAJA45-88-C-0007
8c. ADDRESS (City, State, and ZIP Code) P.O.B. 160, Warrington, Cheshire, England	10. SOURCE OF FUNDING NUMBERS PROGRAM ELEMENT NO. / PROJECT NO. / TASK NO. / WORK UNIT ACCESSION NO.

11. TITLE (Include Security Classification)
Particulate Ceramic Matrix Composites for High Strain-Rate Performance

12. PERSONAL AUTHOR(S)
D.G. Brandon, Y. Yeshurun, L. Baum and M. Farkash

13a. TYPE OF REPORT	13b. TIME COVERED	14. DATE OF REPORT (Year, Month, Day)	15. PAGE COUNT
Final Technical	FROM Dec. 83 TO Aug. 90	1990/09/30	

16. SUPPLEMENTARY NOTATION
Dynamic properties, Ceramic particulate composites, Oxynitride glass, Silicon carbide

17. COSATI CODES			18. SUBJECT TERMS (Continue on reverse if necessary and identify by block number)
FIELD	GROUP	SUB-GROUP	

19. ABSTRACT (Continue on reverse if necessary and identify by block number)

Oxynitride glasses have promising dynamic properties for ballistic applications, notably both a high impedance and a high Hugoniot elastic limit (HEL). The compatibility of these glasses with non-oxide filler materials was investigated, in particular their reaction with B_4C, TiB_2 and SiC. Only SiC was found to be inert at the glass-forming temperature, and 50mm diameter samples for planar impact experiments were hot-pressed with approximately 50 wt% 600 grit SiC powder. These samples contained less than 2% porosity. The filler powder was completely wetted by the glass matrix and homogeneously dispersed in the matrix. No traces of crystalline phases other than SiC were detected. Both the static and the dynamic mechanical properties were determined. The ballistic impedance was approximately that expected from the law of mixtures, while the HEL was close to that of the parent glass.

20. DISTRIBUTION/AVAILABILITY OF ABSTRACT	21. ABSTRACT SECURITY CLASSIFICATION	
☐ UNCLASSIFIED/UNLIMITED ☐ SAME AS RPT. ☐ DTIC USERS		
22a. NAME OF RESPONSIBLE INDIVIDUAL	22b. TELEPHONE (Include Area Code)	22c. OFFICE SYMBOL

DD Form 1473, JUN 86 *Previous editions are obsolete.* SECURITY CLASSIFICATION OF THIS PAGE

ABSTRACT

Oxynitride glasses have promising dynamic properties for ballistic applications, noteably both a high impedance and a high Hugoniot elastic limit (HEL). The compatibility of these glasses with non-oxide filler materials was investigated, in particular their reaction with B_4C, TiB_2 and SiC. Only SiC was found to be inert at the glass-forming temperature, and 50mm diameter samples for planar impact experiments were hot-pressed with approximately 50 wt% 600 grit SiC powder. These samples contained less than 2% porosity. The filler powder was completely wetted by the glass matrix and homogeneously dispersed in the matrix. No traces of crystalline phases other than SiC were detected. Both the static and the dynamic mechanical properties were determined. The dynamic impedance was approximately that expected from the law of mixtures, while the HEL was close to that of the parent glass.

KEYWORDS: Oxynitride glasses, particulate ceramic composites, dynamic properties, planar impact.

CONTENTS

1. Scientific Background 3
   1.1 Ceramics For Ballistic Applications 3
   1.2 Oxynitride Glasses 6
2. Experimental Methods 7
   2.1 Materials 7
   2.2 Powder Preparation 9
   2.3 Hot-pressing 9
   2.4 Microstructural Characterisation 10
   2.5 Mechanical Properties 10
   2.6 Planar Impact Tests 11
3. Results 12
   3.1 Hot-pressing of Particulate-filled Glass 12
   3.2 Microstructural Stability 14
   3.3 Mechanical Properties of Selected Compositions 14
   3.4 Dynamic Properties of SiC-filled Oxynitride Glass 15
4. Discussion 16
5. Conclusions 17
6. References 18

TABLES

1. Properties of some ceramic armour materials. 5
2. Potential oxynitride glasses 8
3. Powder suppliers and properties 8
4. Plates prepared for ballistic tests 13
5. Mechanical properties of particulate composites 15

ILLUSTRATIONS

Fig.1 Projectile and target assemblies and target recovery system for a planar impact experiment. 19

Fig.2 Calculated strain history for a planar impact experiment showing the compressive and release wave fronts. 19

Fig.3 Hugoniot curve for B_4C plotted as pulse pressure against volume strain and compared with the material response to hydrostatic pressure. 20

Fig.4 As-received SiC powder grades. 21

Fig.5 As-received TiB_2 powder grades. 22

Fig.6 Hot press assembly. 23

Fig.7 Geometry of test bars for mechanical testing and definition of parameters. 24

Fig.8 Impact test specimen configurations showing manganin gauge emplacement. 24

Fig.9 Expected manganin gauge signal from the back-surface configuration in the absence of spalling and as a function of the spall strength. 25

Fig.10 X-ray diffraction (XRD) spectrum from glass showing absence of crystalline phases. 25

Fig.11 XRD spectrum from sample with 20 wt% TiB_2. 25

Fig.12 Recorded hot-pressing cycles. 26

Fig.13 Distribution of SiC particles. 27

Fig.14 XRD spectrum from specimen containing 60 wt% TiB_2. 28

Fig.15 Transmission electron micrographs (TEM) of crystalline phases in TiB_2-containing specimens. 28

Fig.16 XRD spectrum of SiC-containing glass showing evidence of $Y_2Si_2O_7$ precipitation. 30

Fig.17 TEM bright field and dark field images of Al_2SiO_5 in specimen with SiC filler. 30

Fig.18 Fracture surface of specimen containing 15 wt% of coarse grained SiC filler powder. 31

Fig.19 Pulse record from a 'back-surface' gauge impact test. 31

Fig.20 Hugoniot curve for the particulate composite compared with that of the oxynitride glass and that of 99.9% Al_2O_3. 32

1. SCIENTIFIC BACKGROUND

1.1 Ceramics For Ballistic Applications

In 1918 it was reported that a 1/16 inch of hard enamel could improve the resistance to bullet penetration of a steel sheet. However, it was not until World War II that the potential advantages of including a hard, ceramic component in an armor system were generally recognised. Plate glass, backed by fibreglass-filled nylon (known as Doron), was introduced in 1945. This lightweight composite armor combination was shown to be capable of stopping rifle bullets. In 1962 Doron-backed alumina panels were found to stop .30 armor-piercing projectiles at half the armor weight per unit area which was required for conventional steel armor. A systematic study of the ballistic performance of a wide range of ceramics subsequently led to the introduction of alumina and boron-carbide armor components during the Vietnam conflict. This was used for the protection of low flying helicopters and their crews. The search for more effective ceramic armor materials continues to the present day [1].

The performance of an armor system is measured in terms of the weight per unit area required to defeat a defined threat from a projectile. The level of threat varies, from low velocity shell fragments and projectiles, through armor-piercing, high velocity bullets, to shaped-charge weapons (which generate a fine, high velocity jet of metal) and long, heavy-metal projectiles. These levels of threat are termed "light", "medium" and "heavy", respectively, corresponding to the increasing kinetic energy of the projectiles. Typically, armor protection for individuals (personnel armor) is only intended to defeat light threats, since the weight of armor which an individual can comfortably carry is strictly limited. Armor carried by military vehicles (armored personnel carriers, for example) is intended to defeat medium threats, such as the .50 armor piercing projectile. Finally, the armor for main battle-line tanks is intended to withstand the heavy threats posed by shaped-charge weapons, such as the various forms of rocket propelled grenades (RPG), and long-rod, heavy-metal penetrators (which may travel at velocities exceeding 1500 $m.s^{-1}$).

The measure of performance generally used to rank armor systems is the V_{50} ballistic test. V_{50} is the velocity of the projectile which will have a 50% probability of penetrating the armor at a fixed angle of incidence. Typically the requirement is for a weight per unit area of armor which will guarantee a given minimum value of V_{50} when tested against a specific projectile. While the V_{50} test serves well to evaluate the effectiveness of an armor system, it does not differentiate well between armor materials [2].

The ballistic performance of ceramic materials can be evaluated by mounting them on a thick metallic block (usually an aluminum alloy) and measuring the depth of penetration of a test projectile travelling at a standard velocity. The thick metal block ensures that the ceramic does not fail prematurely during penetration, so that the reduction in kinetic energy of the projectile by the

ceramic is maximised. The slope of a plot of the residual penetration into the metal backing block as a function of the thickness of the ceramic front plate is generally a straight line, the slope of which can be normalised with respect to density to yield a figure for "ballistic efficiency".

Three main damage regimes exist in ceramics subjected to high strain-rate impact. At low projectile velocities fracture in brittle materials is well described by linear elastic fracture mechanics. As the projectile velocity approaches the sonic velocity (of the order of 500 $m.s^{-1}$, corresponding to strain rates of the order of 10^3 s^{-1}), the loading history becomes dominated by shock wave propagation and inertial effects become important. The transition to the third regime occurs when the damage becomes dominated by the adiabatic response of the target, which can lead to melting and, for very high impact energies, vaporisation at the point of impact [3].

In assessing the high strain-rate performance of ceramics for armor applications, it is the response to a shock wave which is in most cases decisive [4]. To determine this response, a lapped target plate of the ceramic under test is subjected to planar impact by a projectile accelerated to a known velocity (Fig.1). The planar geometry allows the material response to be plotted in two dimensions on a distance-time plot (Fig.2). At the moment of impact, planar compressive shock waves are propagated from the surface of contact into both the target and the projectile. In the elastic regime, the pressure generated in a compressive shock wave is linearly proportional to the material particle velocity, the constant of proportionality being known as the elastic impedance. The impedance is equal to the product of the density and the shock wave velocity, while the particle velocity is equal to the velocity of the contact surface. The ratio of the particle velocity to the shock wave velocity is thus equal to the elastic strain generated by the shock wave (compare Fig.2). Since planar shock waves propagate in one dimension only, there are no dimensional changes perpendicular to the direction of propagation, so that the elastic strain perpendicular to the wave front is equal to the volume strain in the material. The compressive shock waves are eventually reflected as tensile release waves from the back surfaces of both target and projectile. These cancel the compressive stress in the material. A tensile stress is only produced if the release waves from the target and the projectile can act to reinforce each other. This is the situation in Fig.2, for which the target thickness is much greater than that of the projectile. The tensile stress can give rise to fracture by delamination in the plane in which the release waves first overlap - a failure mode which is called "spalling" and is also illustrated in Fig.2.

The dependence of the material particle velocity on the compressive impact pressure is termed the "Hugoniot" and is a characteristic of the material. A typical curve for a ballistic ceramic is shown in Fig.3. The curve is the dynamic equivalent of a static stress-strain curve, in which the elastic impedance governs the initial slope of the curve in place of the elastic modulus. Like a stress-strain curve, the region of elastic

response is terminated at a critical pressure, termed the "Hugoniot elastic limit" (HEL), at which the material starts to undergo irreversible shear. Above the HEL the Hugoniot approaches and becomes parallel to a pressure response curve, the "hydrostat", typical of the liquid state (which has no shear strength, see Fig.3). In metals the HEL is the critical pressure for the onset of plastic yielding, and is generally low compared to the spall strength of the metal (usually determined from the material response to the subsequent tensile history of the stress pulse). In ceramics, on the other hand, the HEL is very much higher than the spall strength, which usually falls to zero as the compressive pulse pressure approaches the HEL. This is in line with the static behaviour of ceramics, which have excellent compressive strengths but are very weak in tension. The dynamic properties of major importance in the selection of ceramic armor materials are the elastic impedance and the HEL. Other material properties of significance are the density, the elastic modulus and the static compressive strength or hardness. However these properties are themselves related to the dynamic properties. Ceramics with high impedance and high HEL in general exhibit high modulus, high compressive strength or hardness and high density. For example, in the case of boron carbide, the low density is more than compensated by the very high modulus and hardness, to give a material with excellent ballistic properties.

The relevant properties for some ceramics which have been proposed for armor applications are listed in Table 1. Nearly all successful ceramic armors have been dense, single phase, monolithic materials. Two-phase mixtures and porous ceramics have proved markedly less successful. This is assumed to be connected with the high internal stresses generated at the interface between two phases of different impedance [5].

Table 1
Relevant Properties of Some Candidate Materials for Ceramic Armor

Material	Density	Shock wave velocity		HEL	Elastic impedance
	g/cm^3	C_1	mm/μsec	GPa	$MPa.s.m^{-1}$
Alumina	3.92		10.7	11	42
Boron carbide	2.50		13.7	15	34
Silicon carb.	3.20		13.1	9.6	42
Ti.diboride	4.52		11.3	11	51
Al.nitride	3.25		10.2	7.2	33

A major problem in the use of ceramic armor is the extent of the damage zone accompaning a primary hit. Radial and spall cracks propagate through the ceramic outward from the site of impact, leading to fragmentation of the ceramic. Such damage can to some extent be reduced by increasing the rigidity of the backing plate, in order to limit the bending stresses generated during impact. Ultimately, however, it is neccessary to improve the resistance of the ceramic to crack propagation, that is, to increase the fracture toughness of the ceramic. If this can be successfully achieved, then the area of damage around the impact

point will be reduced, and the ability of the ceramic armor to withstand a second hit can be improved. At present, the accepted method of limiting the size of the damage zone is to reduce the initial size of the tiles. Since this introduces edge effects, which reduce the ballistic efficiency, an improvement in the toughness of the ceramic would be very desirable.

In addition to ceramic armor, several attempts have been made to introduce glasses into armor systems. The primary disadvantages of glass are their low elastic modulus (which reduces their impedance) and fracture toughness when compared to crystalline ceramics. This is partly compensated by the lower density of the more open amorphous structure, but a more important effect is an elastic softening which has been observed in some glasses subjected to high pressures. This leads to a curvature of the Hugoniot in the elastic region which is the inverse of that usually observed (an increase in the tangent modulus at high pressures) and results in dispersion of the primary shock wave.

Nitrogen containing glasses are of particular interest, since they have been found to have a comparatively high elastic modulus [6]. Furthermore, nitrogen glasses based on yttria additions also have higher densities, so that they offer a possibility of achieving a reasonable impedance match with conventional ballistic ceramics. Finally, the Hugoniot curve for selected oxynitride glasses has been determined by the authors and the value of the HEL was found to be exceptionally high and well into the range considered desirable for ceramic materials intended for high strain rate applications [7].

1.2 Oxynitride Glasses

The basic problem associated with the preparation of oxynitride glasses is the suppression of the evolution of nitrogen gas during melting of the glass [8]. This can be achieved by applying an overpressure of nitrogen, by adding free silicon metal to the glass, or by adding stabilising oxides (especially Y_2O_3) [9, 10]. Nitrogen contents of a few percent are quite stable at normal glass melting temperatures, but the viscosity rises rapidly with nitrogen content, and glass melting at nitrogen contents exceeding 10 at.% is only possible at temperatures exceeding 1700°C [8, 9]. While 5 wt.% of silicon metal is sufficient to suppress nitrogen evolution at atmospheric pressure from a MgO containing glass, nearly 50 wt% of Y_2O_3 is required to suppress nitrogen evolution in nitrogen glasses containing 6 to 15 at.% nitrogen.

The elastic properties of yttria-based oxynitride glasses were determined by Messier [6], who also confirmed that the materials remained free of crystalline phases for nitrogen contents of up to 15 at.%. The elastic modulus was found to increase from 141 GPa at 6.3 at.% nitrogen to 186 GPa at 15.0 at.% nitrogen. The density of these yttria-containing compositions varied from 3.82 to 4.0 $gm.cm^{-3}$. The mechanical impedance is thus some 50% less than that of a good ballistic alumina. This may be compared to a normal borosilicate glass, with a density of 2.55 and an elastic modulus

of 60 GPa, corresponding to an impedance one third that of alumina and only half that of the oxynitride glass compositions.

The authors determined the Hugoniot curves of two oxynitride glasses prepared by Messier and confirmed their high impedance. Moreover, the values of the HEL were found to be 9.0 and 10.4 GPa for the 6.0 and 13.3 at.% nitrogen glasses respectively, comparable to the HEL of a high purity alumina [4]. Finally, the measured stress signals in the high stress range showed that the transmitted compressive shock waves were composed of an initial elastic jump followed a slower, 'plastic' wave. This behaviour is indicative of some dispersive behaviour not normally seen in a ceramic target. In addition, the estimated spall strength for both glass compositions was of the order of 0.8 GPa, decreasing to zero at the HEL. This is higher than the spall strength reported for alumina ceramics (0.3 to 0.4 GPa) [5].

A major factor in the development of ballistic ceramics is the effect of impedance mismatch at internal boundaries on the ballistic properties [15]. In general, shockwaves are expected to be scattered by all such boundaries, leading to the development of high internal stresses. These internal stresses will lead to cumulative damage and eventual failure. For this reason, monolithic, single-phase ceramics have been the materials of first choice for high strain-rate applications. For the same reason, residual porosity is regarded as a major microstructural defect, since a pore is the most effective microstructural feature for the scattering of a shockwave. On the other hand, the presence of a second phase may serve to improve the microstructural homgeneity and inhibit undesirable grain growth, so that it is not immediately obvious that the addition of the second phase is necessarily deleterious to the dynamic properties. In the case of an oxynitride glass, the addition of a ceramic filler material with a suitably matched impedance may be expected to improve the toughness, while the ballistic properties (the HEL and the spall strength) remain uneffected. It is to verify these expectations that the present project was undertaken.

2. EXPERIMENTAL METHODS

2.1 Materials

The compositions and properties of the oxynitride glasses investigated by Messier are given in wt.% in Table 2 (note that the compositions in the original publication are given in terms of the at.% of the elements). Of these compositions, only those labelled 'a' and 'b' were studied in the present programme, since these were the compositions whose Hugoniot had been studied previously.

Table 2 - Potential oxynitride glasses.

wt.%	'a'	'b'	'd '	'h'
Al_2O_3	11.5	23.83	11.32	17.25
Si_3N_4	7.91	16.39	31.39	17.80
SiO_2	30.06	7.02	6.77	7.63
Y_2O_3	50.53	52.77	50.52	57.32
(N)	3.16	6.56	12.56	7.12
X-ray diff.	amorph.	amorph.	some β-Si_3N_4	amorph.
Density, $gm.cm^{-3}$	3.82	3.92	3.92	4.00
Modulus, GPa	141	157	183	186

Three ceramic filler materials were considered for these glasses: B_4C, SiC and TiB_2, these being the three non-oxide monolithic ceramics with the best known high strain-rate performance. In order to determine the effect of filler particle size, more than one grade of the two fillers SiC and TiB_2 was used.

All materials were obtained as powders, for which the relevant details are given in Table 3.

Table 3 - Powder Suppliers and Properties.

Powder & Grade	Supplier	Particle size, µm	Purity %
Al_2O_3 (A16)	ALCOA, USA	1.0	99.5
$SiO_2.nH_2O$	J.T.Baker Chemical Co., USA	-	99.87
Si_3N_4 (H1)	Hermann C.Starck, FRG	<0.8	98.07
Y_2O_3 -	Alpha Products, USA	4	99.99
B_4C -	Union Carbide, USA	4.5	99
SiC (HSC059)	Superior Graphite Co., USA	<2	99.05
SiC (HSC077)	Superior Graphite Co., USA	<15	96
TiB_2 -	Union Carbide, USA	3	99.5
TiB_2 (HPU)	Adv. Refrac. Tech., USA	3.7	99.06
TiB_2 (HPF)	Adv. Refrac. Tech., USA	6.0	99.54

The powder morphologies were checked by scanning electron microscopy. While the details of the powder morphology are not particularly relevant for the powder constituents of the oxynitride glass, the filler powder morphologies are expected to have some bearing on the properties of the final product. Fig.4 shows the two grades of SiC powder. A wide range of particle size is clearly evident, especially in the finer, HSC059 grade. Further more, the particles have the jagged surface morphology associated with a ground product. For comparison, Fig.5 shows two of the grades of TiB_2, both of which were expected to have roughly the same particle size. In this case, one of the grades (HPF) was found to contain a small proportion of very coarse grains, up to 30µm in diameter - an obviously undesirable feature. Otherwise, the grain size distribution was comparatively narrow and the individual grains exhibited well-developed crystal facets. It

proved impossible to prepare B_4C-filled composites (see below), so that the powder morphology of B_4C is irrelevant.

2.2 Powder Preparation

The constituent powders for the oxynitride glass were milled in deionised water at 20 to 30 vol% solids loading using a heavy duty batch attrition mill (Union Process, Akron, Ohio; model 01-HD). The powder mix was milled for two hours at 400 to 500 rpm using 1/8in. diameter alumina milling beads with a media/slurry ratio of approximately 1:1. The filler powders were also dispersed in deionised water at 50% solids loading with the aid of a high-intensity ultrasonic probe (Sonics and Materials, Inc., Danbury, Connecticut; model VC-600) and stabilised by the addition of a small amount of commercial dispersant. The two slurries were then blended by ball-milling for a further three hours, again using alumina milling media. No especial control or adjustment of pH was found to be necessary. Foaming of the filler slip during ultrasonic dispersion could be suppressed by degassing prior to dispersion in a vacuum dessicator. The batch size was dictated by the capacity of the attrition mill (250cc).

The blended slip was cast onto a plaster base and allowed to dry. The green product was passed through a 20 mesh sieve and the resulting free-flowing granules were cold-compacted at 50MPa. All the process development studies were conducted on 30mm diameter discs, approximately 7mm in thickness. This was upgraded for the final planar impact ballistic tests to 50mm diameter discs.

2.3 Hot-Pressing

The hot-press assembly was constructed in-house and is shown in Fig.6. This assembly has been considerably modified during the course of the programme. In the final version, the press can be operated at temperatures of 1850°C and pressures of up to 50MPa. The induction generator has a capacity of 30Kw, but the final version of the system typically required 4-5Kw to reach the peak temperature. The carbon black insulation provides a measure of environmental protection, but no attempt was made to provide an inert gas shield.

Temperatures up to 1400°C were monitored by a platinum/platinum-rhodium thermocouple inserted into a cavity in the top (stationary) plunger. Temperatures from 1200°C were measured with an optical pyrometer sighted on a hole in the graphite press which terminated at the inner graphite sleeve. In the region of overlap the thermocouple typically gave the lower reading (by about 100 to 160°C). This is thought to reflect a real difference in temperature between the centre portion of the press (where the pyrometer was sighted) and the bottom of the top plunger (where the thermocouple rested against a graphite spacer).

Pressure was monitored by a simple pressure dial gauge mounted on a hand-operated hydraulic jack used to raise the lower plunger. The primary advantage of applying the pressure by raising the

lower piston is a more uniform pressure distribution in the die cavity than could be obtained by pushing down on the upper plunger, since the die body is less restricted. The displacement of the piston of the hydraulic jack was read off from a micrometer dial gauge attached to the mainframe of the press. The mainframe was water-cooled to minimise dimensional changes and was designed for operation at up to 15 tons. In addition to split graphite sleeves, the die cavity was protected by a grafoil sleeve, boron nitride powder and graphite and grafoil spacers between the disc specimens. Three disc specimens have been successfully pressed simultaneously in a stack, but in the case of the final, 50mm diameter discs only two were prepared in any given run. The specimens were identified by their run number and their position in the stack. Specimens for the current project were identified by the prefix 'SYN'.

2.4 Microstructural Characterisation

Specimens for both microstructural characterisation and mechanical testing were prepared by diamond grinding and diamond disc cutting. An automated slicing unit (Meyer & Burger, Switzerland, model TS33) was available for the accurate dimensioning of specimens. Preparation of samples for microstructural analysis included lapping and diamond polishing (to 0.1µm diamond paste), as well as sputter-gold coating of specimens for scanning electron microscopy (SEM). Specimens for transmission electron microscopy (TEM) were prepared by 'dimpling', ion-milling (Gatan twin milling unit) and carbon coating. The 3mm diameter TEM specimens were first given a dished cross-section in the dimpler and then argon ion-milled in a rotating holder at a sputtering angle of 12 to 17° to the point of perforation. This was followed by vacuum evaporation of a thin, conducting carbon film to prevent charge build-up in the electron microscope.

SEM examination was performed in a JEOL JSM840 microscope equipped with energy dispersive spectroscopy (EDS) facilities for microanalysis (Link, UK). The TEM specimens were examined in a JEOL JEM120CX instrument operated at 100kV. X-ray diffraction analysis was performed on an automated Philips unit (model PW-1730) equipped with computer software for phase identification. Optical microscopy was performed in conventional reflected light using a Zeiss Axiophot. No especial coating or treatment of the polished specimens was found to be necessary to develop image contrast in the optical microscope.

2.5 Mechanical Properties

The geometry of the test bars used for modulus of rupture (MOR) and single edge-notched beam (SENB) fracture toughness (K_c) tests is shown in Fig.7. A square cross-section (b=d) was used to facilitate testing both parallel and perpendicular to the direction of hot-pressing, even though this leads to a small systematic error in the results. The SENB test was selected for ease of specimen preparation and overall reliability (less than

10% variance). All MOR test specimens were corner ground (1mm flat) and finished by surface grinding parallel to the specimen length with 600 grit silicon carbide powder, in accordance with standard procedures. After fracture toughness testing the two halves of the SENB specimen were used to provide further MOR data.

All mechanical tests were performed on an Instron (model 1195) screw-driven tensile testing machine using a three-point bend jig made from hardened 3340 steel. The MOR and K_c values were calculated from the following formulae:

$$MOR = 3PL/(2bd^2)$$

$$K_c = 3P(L-1)/(2bd^2).\sqrt{a}[3.86-6.15(a/d)+21.7(a/d)^2]^{1/2}$$

The failure load P was determined from the load-time graph. All the parameters are defined in Fig.7.

Hardness testing and indentation crack tests were performed with a Vickers standard test unit (Wolpert, FRG) at loads P of 5 to 20kgms. Radial crack lengths c were measured at a magnification of x500. The indentation fracture toughness was calculated from the formula:

$$K_{cv} = 0.15(E/H_v)^{1/2}P/c^{3/2}$$

H_v is the Vickers hardness and the constant is that appropriate to the geometry of the Vickers indenter. The elastic modulus E was estimated from the previously measured elastic modulus of the oxynitride glass [6] and the catalogue values given for the filler materials by using the rule of mixtures (that is, by assuming that the modulus is a linear function of the volume fraction of the filler). In general, the indentation cracks were less than the minimum length required to characterise K_{Ic}, so that the indentation toughness is expected to under- estimate the true, plane strain fracture toughness.

2.6 Planar Impact Tests

The planar impact experiments were conducted in a 2.5in. gas gun described elsewhere [11]. Impact velocities were measured to an accuracy of ±0.5% and ranged between 100 and 700 $m.s^{-1}$, corresponding to shock pressures in the range 2.5 to 12.0 GPa for a copper impactor. The manganin gauges (M.M., type LM-SS-125cH sp60) were previously calibrated under both loading and unloading conditions [12, 13]. These references also give details of gauge emplacement and data reduction proceedures. The gauges are grid-like foils 0.5µm thick deposited on 0.04mm epoxy sheet. The gauges were either glued between two lapped plates of the oxynitride glass composite, as shown in Fig.8 (a), or between a single disc of the composite and a poly(methyl-methacrylate) (PMMA) backing plate, as shown in Fig.8 (b). In the first configuration, designated 'in-material', we obtain points on the Hugoniot curve, while from the second, 'back-surface'

configuration we are also able to evaluate the spall-strength and the HEL of the specimens.

The basic principles involved in measuring the spall strength of shock-loaded specimens using manganin gauges were described previously [14] and possible effects are shown schematically in Fig.9, which illustrates the expected behaviour for zero spall strength, for a finite spall strength and for no spalling.

3. RESULTS

3.1 Hot-pressing of Particulate-filled Glass

Burn-off of the organic additives in a hot-pressing run was complete by the time the temperature reached 500°C, at which time a pressure of 10 to 15MPa was applied. Compaction was found to initiate at between 900 and 1100°C, with the onset of glass formation, and the displacement of the piston was monitored as compaction proceeded. The final compaction temperature was between 1350 and 1600°C, depending on the filler content of the glass and the compaction pressure. The processing window was defined by the onset of nitrogen gas evolution at high temperatures and the failure of the material to sinter if the temperature was too low. In effect, the lower limit of temperature is determined by the rate of glass formation, which is also a function of the soaking time. In the present work the soaking time at maximum temperature was varied from 15 to 60 minutes.

In the first instance, the glass compositions 'a ' and 'b' were prepared and compacted without filler additions. Both compositions exhibited excessive fluidity (in the absence of filler powder) above 1500°C (nominal temperature), while glass formation was incomplete below 1400°C, as demonstrated by XRD. On the other hand, the 'b' composition was found to contain gas bubbles at all temperatures for which glass formation was complete. For this reason, all subsequent work was concentrated on composition 'a', and the final soaking temperature was generally restricted to the range 1400 to 1450°C. In the absence of filler powders, this resulted in a 100% glassy material, as demonstrated by the XRD spectrum, Fig.10.

The addition of B_4C filler powder to the glass composition resulted in extensive gas evolution during hot-pressing associated with a strong reaction between the filler powder and the glass. The highly porous compact resulting from this reaction was considered as clear indication that the filler was incompatible with the glass composition, and attempts to use B_4C as a filler were therefore abandoned.

In the case of TiB_2 additions, good densification was obtained for pressing temperatures of 1350°C and above, but at the lower pressing temperature glass formation was incomplete and residual crystalline phases were present. On the other hand, while pressing at higher temperatures (1400 to 1450°C) was expected to lead to complete formation of the glass with no crystalline phases other than TiB_2, in practice secondary phases were observed (Fig.11)

which are associated with a reaction between the filler and the glass (see below). It was concluded that although TiB_2 could be used as a filler without having a deleterious effect on the final density, nevertheless it was not suitable for the purposes of the current investigation.

Additions of SiC of between 15 and 60 vol.% were made to the 'a' composition oxynitride glass and hot-pressed at temperatures of 1350 to 1600°C. As with the previous fillers, glass formation was incomplete at the lower end of this range, but in contrast to the other fillers, no evidence for any secondary reactions was observed at the higher temperatures. However, the material containing 60 vol.% filler was found to contain approximately 6% residual porosity. It was therefore decided to prepare the 50mm diameter planar impact test specimens from a single composite composition comprising 50 vol.% SiC. Furthermore, the grade of SiC selected for the final composition was HSC059, since the mechanical properties were appreciably better than those obtained with the HSC077 grade, even though the distribution of the grainsize was far more uniform and narrow than that of the HSC059 grade (see below). The hot-pressing temperature for these larger discs was approximately 1600°C.

The initial attempts at hot-pressing the larger discs yielded specimens which were radially cracked. These processing defects were eventually traced to sintering stresses developed during the heating cycle. In effect, the sintering rate exceeded the rate of flow in the die, leading to tangential stresses which are a maximum at the periphery of the disc. Reducing the heating rate to less than 4°C/min. in the critical temperature range (1100 to 1400°C) eliminated the problem. Examples of the recorded hot-pressing cycles for both the original (fast) cooling rate and the revised (slow) cooling rate are given in Fig.12. The final discs were free of residual crystalline phases other than the filler and had porosities of 4% or less (see Table 4).

Table 4 - Plates prepared for ballistic tests.

Designation	Density	%Theoretical	Radial Cracks
18A	-	-	broken
18B	3.37	95.0	none
19A	3.42	96.3	none
19B	3.43	96.6	large
19C	3.42	-	large
20A	3.44	96.9	none
20B	3.43	-	large
21A	3.42	96.3	small
21B	3.41	96.2	small
22B	3.42	96.3	none
23A	3.40	95.9	none
23B	3.40	95.9	none
23C	3.42	96.4	none
23D	3.41	96.2	none
23E	3.41	96.2	none

3.2 Microstructural Stability

As noted above, the boron carbide filler was inherently unstable in the oxynitride glass, presumably oxidising to B_2O_3 and releasing gaseous CO. The silicon carbide filler, on the other hand, appeared to be stable at the glass-forming temperatures with no evidence of any dissolution in the glass matrix or of the formation of additional crystalline phases. The filler appeared to be well-dispersed, although there was a rather wide distribution of particle size. Finally, TEM examination indicated that the glass matrix had had no effect on the particle morphology (Fig.13).

The behaviour of TiB_2 as a filler material was different again. In this case additional phases were observed to form at pressing temperatures in the glass forming range. Unexpectedly, none of the minor phases appeared to contain titanium. Some of the phases, which were clearly present as extra lines in the XRD pattern, Fig.14, were identified by TEM as Si_2ON_2, $YAlO_3$ and $Y_4Al_2O_9$, Fig.15. Other lines in the XRD pattern could have been associated with titanium compounds such as $Al_{24}Ti_8$ or $Ti_7Al_5Si_{12}$, but this should be confirmed by TEM. It is not at all clear why the presence of TiB_2 should stabilise titanium-free phases.

An attempt was made to follow the progress of glass formation in filler-free specimens as well as in specimens containing the SiC filler. In general, crystalline silicates of both yttria and alumina were observed to form in the early stages of glass formation, for example $Y_2Si_2O_7$ (identified by XRD, Fig.16) and Al_2SiO_5 (identified by TEM, Fig.17). In addition β-Si_3N_4 was occasionally observed, indicating that the α to β transformation, which is generally agreed to occur by precipitation from a glassy phase, could occur under the present processing conditions. In practice it is probable that most of these transitory phases are associated with local compositional inhomogeneities. In any event, during hot-pressing considerable shear must take place to accomodate the volume change in the die, and these local inhomogeneities are unlikely to persist in the final product.

3.3 Mechanical Properties of Selected Compositions

The strength (MOR), hardness and toughness of the oxynitride glass were all found to be greatly improved by the addition of filler powder. Representative values are given in Table 5 which summarises results for one grade of TiB_2 and both grades of SiC (fine particle size, HSC059, and coarse particle size, HSC077).

Table 5 - Mechanical Properties of Particulate Composites

Filler wt%	26%TiB_2	15%SiC	29%SiC	50%SiC
Part.Size	3μm	‹15μm	‹15μm	‹2μm
Dens.g.cm^{-3}	3.36	3.55	3.53	3.32
MOR MPa	145±17	112±21	174±30	310±50
VHN H_v	870±46	758±27	992±57	1048±55
K_c MPa$\sqrt{m}$	2.5±0.4	2.1±0.4	2.4±0.5	3.9±0.2
E GPa	-	-	-	245

These mechanical properties are far better than could be obtained without the addition of a filler. Although the toughness is low compared to high performance ceramics, it is comparable to that of commercial grades of alumina tiles. Similarly, although the hardness is low it is also comparable to commercial grades of alumina (for example, those containing approximately 90% Al_2O_3). The mechanical strength (MOR) is again comparable to that obtained from a good quality structural alumina tile.

A further indication that the mechanical properties have been greatly improved is provided by the SEM images of fracture surfaces. Fig.18 shows the fracture surface of the composite containing 15% coarse grained SiC. The surface is very rough and shows both cleavage facets in the SiC and river lines in the glassy phase.

3.4 Dynamic Properties of SiC-filled Oxynitride Glass

The 50mm diameter sample plates of the oxynitride glass containing approximately 50 vol% SiC powder filler were tested in planar impact, using both the 'in-material' and the 'back-surface test configurations (see section #2.6).

The 'in-material' configuration provides an accurate measure of the impact pressure and the accompanying particle velocity of the material for any given impactor of known velocity and mechanical impedance. For each projectile velocity, such a test thus gives a point on the Hugoniot curve. The 'back-surface' configuration, on the other hand, is very sensitive to any changes in wave velocity, such as occur at the Hugoniot elastic limit (HEL), above which an elastic precursor wave starts to break away from the slower shock wave associated with propagation at a higher peak impact pressure. In effect, once the peak pressure exceeds the HEL, the material is damaged during shock-wave propagation and the shock-wave velocity is reduced. From the height of the precursor wave observed in the 'back-surface' configuration it is thus possible to measure the HEL accurately, although it is not possible to obtain an accurate measure of the particle velocity in this configuration.

In the present work it has not proved possible to derive any information concerning the spall-strength. Such information is normally obtained from the pull-back signal observed in the 'back-surface' configuration (section #2.6), and no clear pull-back signal was obtained in the present experiments. An example of the signal pulse obtained in the back-surface

configuration is given in Fig.19. This signal was obtained using a copper impactor at a velocity of 615 $m.s^{-1}$. The verticle scale is 0.2 $V.cm^{-1}$ and the horizontal (time) scale is 0.5 $\mu s.cm^{-1}$.

The results of the planar impact tests are summarised in Fig.20, which compares the Hugoniot curve derived for the particulate composite oxynitride glass/SiC specimens with both the Hugoniot derived for the glass alone [7] and the Hugoniot for a high performance alumina (AD 99) [14]. The impedance of the composite is significantly greater than that of the parent glass, and is in fact somewhat higher than would have been expected on the basis of a simple law of mixtures rule. The HEL, on the other hand, is, within experimental limits, identical to that of the parent glass. Since the parent glass wets the SiC filler completely, this latter result is not unexpected.

4. DISCUSSION

This investigation can be divided into three sub-topics:
1. The compatibility of non-oxide ceramic filler powders with yttria-based oxynitride glasses.
2. The development of procedures for hot-pressing planar impact test specimens of particulate ceramic composites based on oxynitride glass.
3. The measurement of the ballistic properties of oxynitride glass matrix particulate composites by planar impact.

The restrictions imposed on the processing route used in the present programme were, principally, the composition of the oxynitride glass and the environment of the hot-press. Thus only the glass compositions previously investigated by Messier were studied, since these were the materials whose ballistic properties were available; while the hot-press was operated at ambient atmosphere (with the partial pressure of nitrogen modified by the generation of CO, associated with oxidation of the carbon black insulation). In particular, it was found that only one glass composition was microstructurally stable, containing 3.16 wt% or 6.3 at% of nitrogen. The higher nitrogen content glass always contained some porosity associated with gas evolution during sintering.

As suspected from the relative thermodynamic stability of the oxides and carbides of silicon and boron, boron carbide was found to be totally unstable under the conditions required for glass formation, while silicon carbide was found to be completely stable. Massive evolution of gas was the primary result of the reaction with B_4C, leading to a completely porous product. No evidence for any reaction with SiC was found, even at the limit of detection in the transmission electron microscope (of the order of 1-2nm).

The reaction of the oxynitride glass with titanium diboride was less expected, although the borides are inherently less stable than the carbides and nitrides of the same metal, while B_2O_3 is, of course, readily formed. Since the reaction products are in this case all solid, the reaction with TiB_2 is not a barrier to the

formation of the particulate composites. It should be noted that the titanium compounds which have been identified are all aluminium containing, consistent with the well known stability of the titanium aluminides and suggesting that an alumina-free glass composition might have been less reactive.

The mechanical properties of both the SiC and the TiB_2 containing composites were satisfactory, but the properties obtained from the material containing 50 vol% of fine grained SiC were far better than expected and were comparable to a good ballistic tile manufactured from a monolithic ceramic.

The development of the powder preparation, hot-pressing and machining procedures for the ballistic tile planar impact test specimens was more difficult than anticipated. This was partly because the batch size for the slip in the attrition mill was limited and partly because the development of sintering stresses resulted in radial cracking of the larger tiles required for planar impact testing. The powder preparation methods finally adopted are given above, while the hot-pressing parameters have been closely specified in order to avoid radial cracking of the discs during heating to peak temperature, achieve full glass formation and prevent excessive glass fluidity. All these problems are essentially technical and have no bearing on the scientific relevance of this project.

As previously noted, the motivation for this project was the excellent ballistic response of the oxynitride glasses observed in earlier planar impact tests. The results obtained with the particulate composite tiles have now demonstrated that these properties are not degraded by the addition of up to 50 vol% SiC filler to the glass composition, while the static mechanical properties have been greatly improved. In effect, the particulate composite has been found to have a ballistic response significantly better than the parent glass, with an impedance in excess of a law of mixtures prediction. At the same time the high HEL of the glass has been maintained, while both the static toughness and the bend strength have been significantly increased over those of the parent glass by the particulate additions.

5. CONCLUSIONS

1. An oxynitride glass containing 6.3 at% nitrogen is incompatible with a B_4C filler powder, reacts significantly with a TiB_2 filler powder and is inert to SiC filler powders at the temperatures required for glass formation.

2. The addition of a SiC filler powder to this same oxynitride glass results in a significant improvement in the modulus of rupture, fracture toughness and hardness of the glass. The maximum improvement in mechanical properties was observed for a 50 vol% particulate composite with a fine grained silicon carbide.

3. Large disc specimens of a particulate, 6.3 at% N, oxynitride glass composite containing 50 vol% SiC can be prepared by hot-pressing free of processing defects provided careful

attention is payed to the powder preparation and hot-pressing parameters.

4. The high strain rate properties of this particulate composite are also either comparable to or better than those of the oxynitride glass matrix without the particulate filler.

6. REFERENCES

1. A.K.Wong & I.Berman,'Lightweight ceramic armor - A review', AMMRC MS 71-1 (1971)

2. D.Viechnicki, W.Blumenthal, M.Slavin, C.Tracy & H.Skeele, 'Armor ceramics - 1987', Proceedings, 3rd TACOM Armor Coordinating Conference, Monterey CA (1987)

3. T.Z.Blazynski, 'Materials at high strain rates', Elsevier Appl.Sci. (1987)

4. L.Davison & R.A.Graham, Phys.Rep.SS 255 (1979)

5. Y.Yeshurun, D.G.Brandon, A.Venkeret & Z.Rosenberg, J. de Phys., 49[C-3], 11 (1988)

6. D.R.Messier & A.Broz, Comm.Am.Ceram.Soc., 65, C-123 (1982)

7. Y.Yeshurun & D.G.Brandon, 'The dynamic response of oxynitride glass', Report to AMTL, Watertown, Dec. 1986

8. R.A.L.Drew, S.Hampshire, and K.H.Jack, 'The preparation and properties of oxynitride glass', Riley F.L. (ed) Progress in Nitrogen Ceramics, Martinus Nijhoff, p.323 (1983)

9. D.R.Messier, Cer.Eng.Sci.Proc., 3, 565 (1985)

10. J.Rocherulle, J.Guyader, P.Verdier & Y.Laurent, J.Mat.Sci., 24, 4525 (1989)

11. Y.Porat & M.Gvishi, J.Phys.E, 13, 504 (1980)

12. Z.Rosenberg, D.Yaziv & Y.Partom, J.Appl.Phys., 51, 3702 (1980)

13. D.Yaziv, Z.Rosenberg & Y.Partom, J.Appl.Phys., 51, 6055 (1980)

14. D.Yaziv, Ph.D. Thesis, Univ. of Dayton, Ohio (1985)

15. Y.Yeshurun, Z.Rosenberg and D.G.Brandon, Proc. 4th Int.Conf. on Mechanical Properties at High Rates of Strain, Oxford 1989, Inst.Physics (1989)

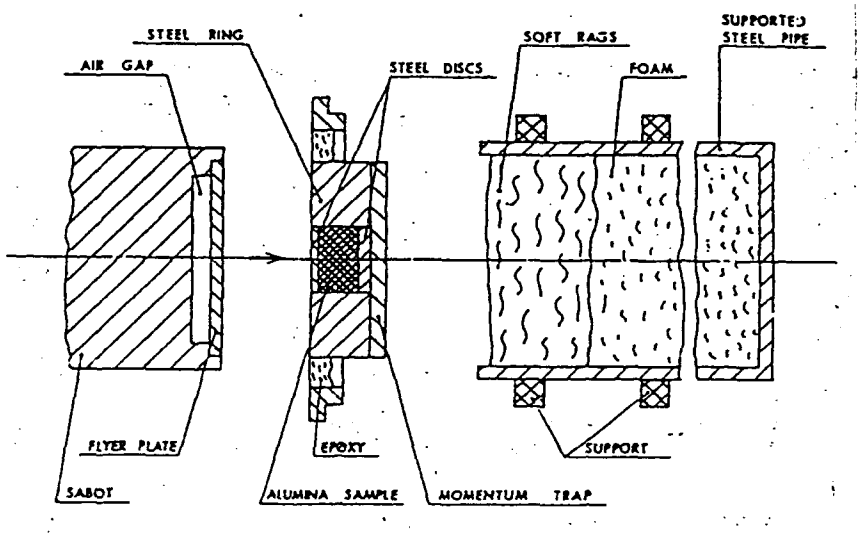

Fig.1 Projectile and target assemblies and target recovery system for a planar impact experiment.

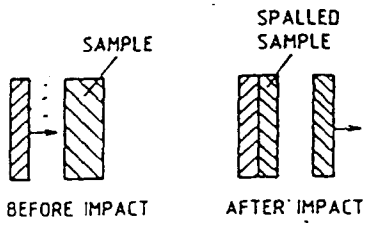

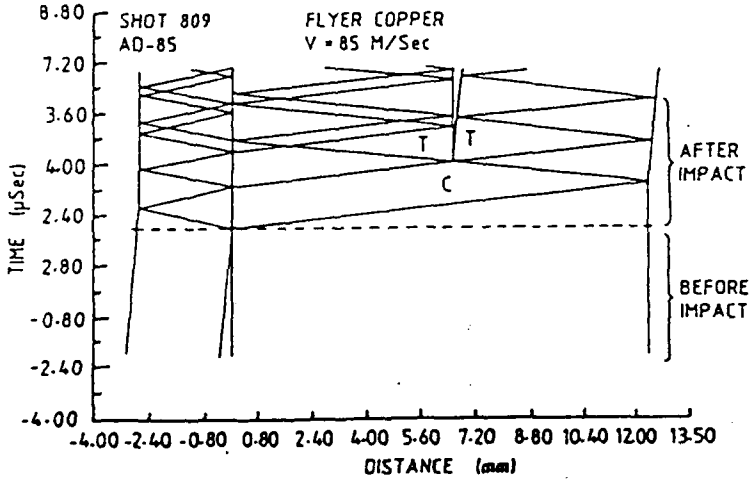

Fig.2 Calculated strain history for a planar impact experiment showing the compressive and release wave fronts. The target is under compression in region C and tension in region T, where spall failure is initiated due to overlap of the two release waves from the back surfaces of the target and projectile.

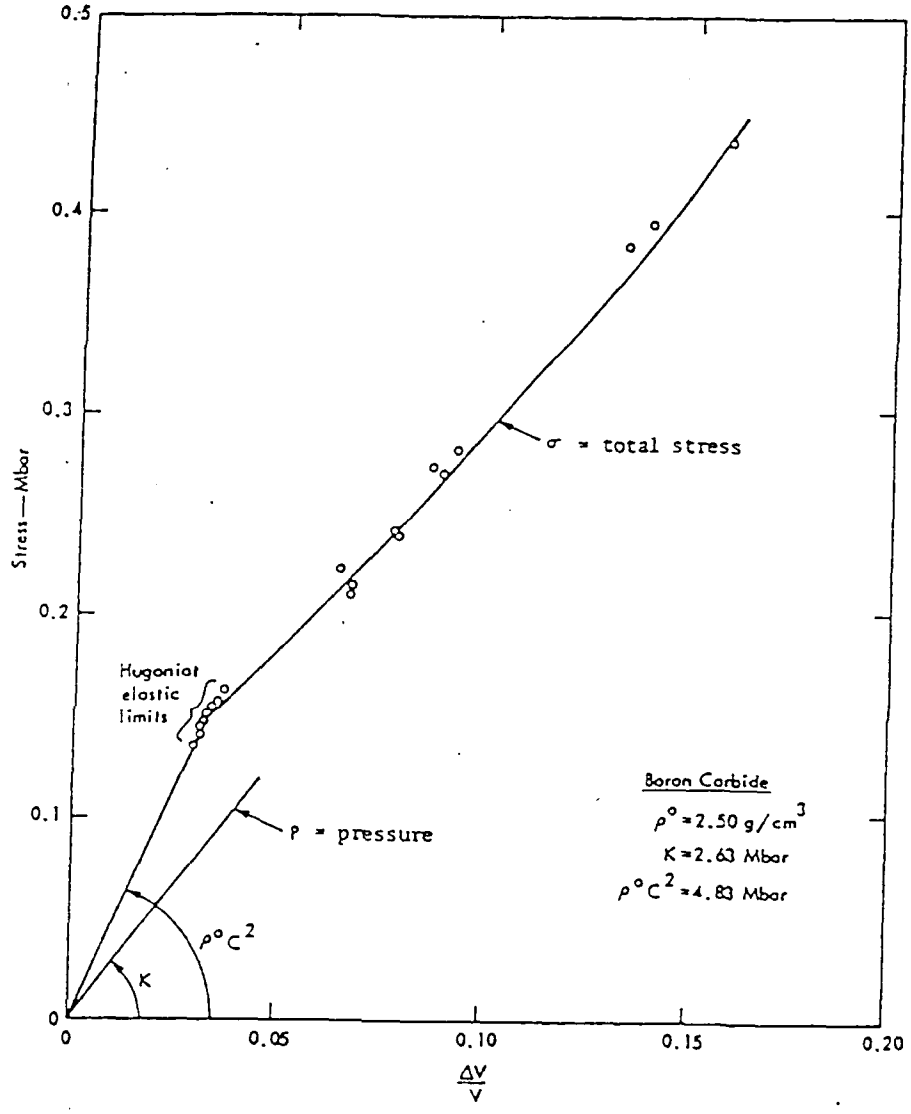

Fig.3 Hugoniot curve for B_4C plotted as pulse pressure against volume strain and compared with the material response to hydrostatic pressure. The volume strain is equal to the ratio of the particle to the shock wave velocity.

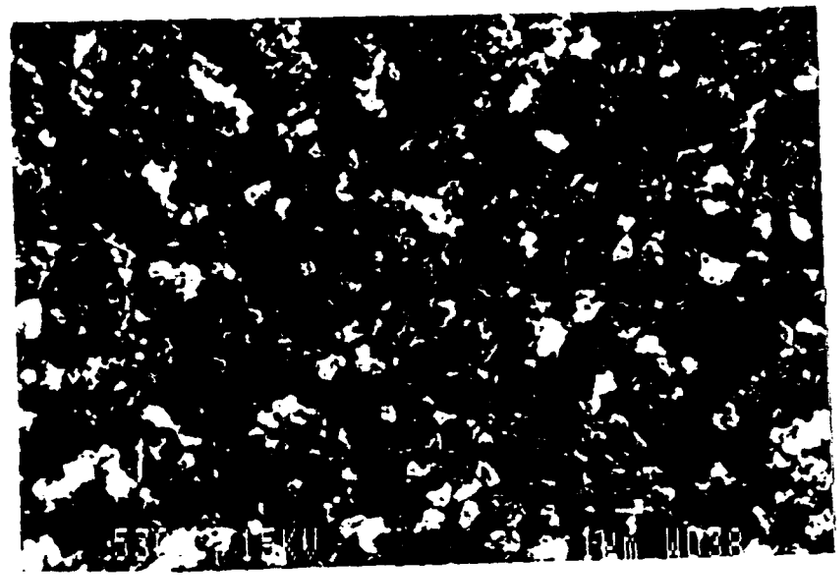

(a) HSC059, particle size ‹2µm

(b) HSC077, particle size ‹15µm

Fig.4 As-received SiC powder grades.

(a) Union Carbide material, avge. particle size 3μm

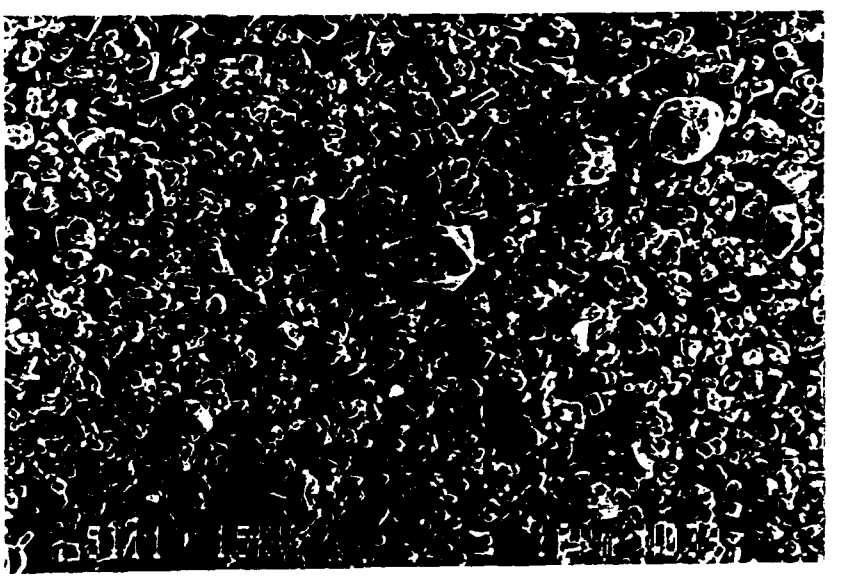

(b) HPF grade, avge. particle size 6.0μm

Fig.5 As-received TiB_2 powder grades.

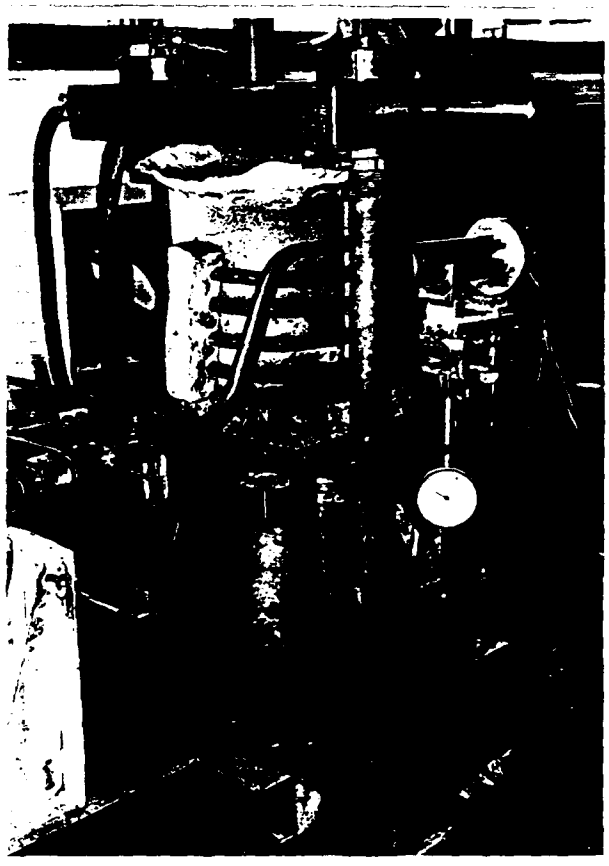

(a) General view showing press (centre), hydraulic jack (below), displacement gauge and pyrometer assembly (above gauge).

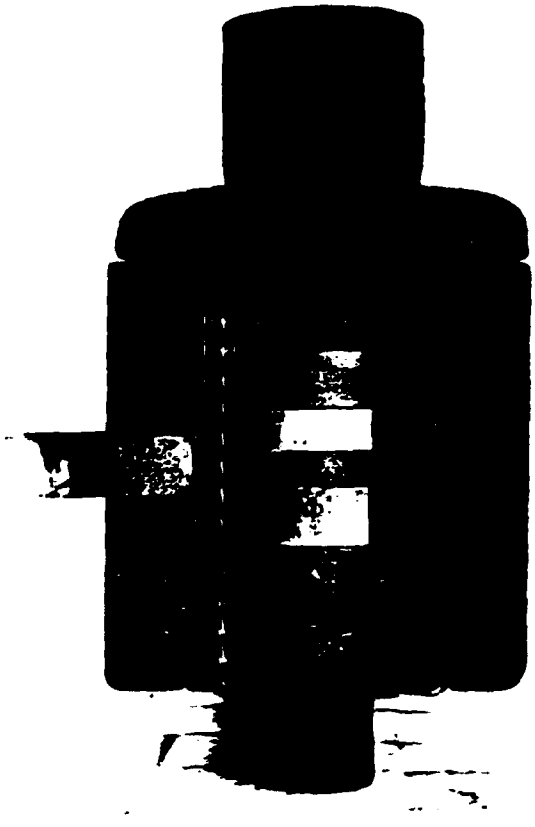

(b) Sample assembly shown mounted in a half-section of the graphite susceptor.

Fig.6 Hot press assembly.

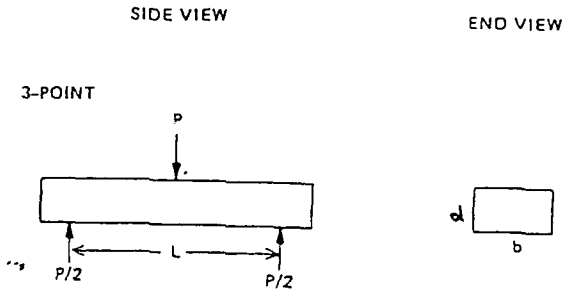

(a) Three-point modulus of rupture (MOR) specimen.

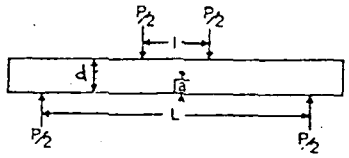

(b) Four-point single edge notched beam (SENB) fracture toughness specimen.

Fig.7 Geometry of test bars for mechanical testing and definition of parameters.

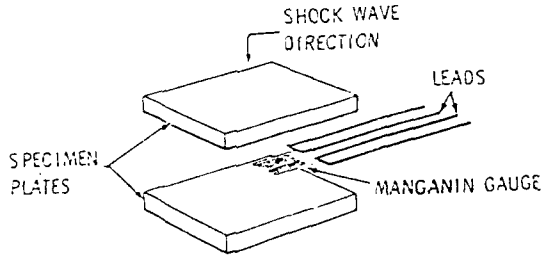

(a) In-material configuration for measurement of the Hugoniot.

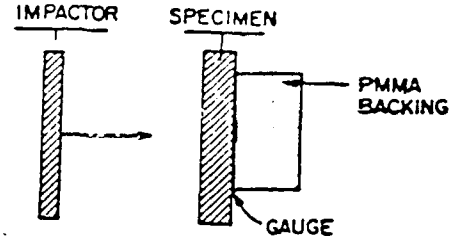

(b) Back-surface configuration for determination of the Hugoniot elastic limit (HEL) and spall strength.

Fig.8 Impact test specimen configurations showing manganin gauge emplacement.

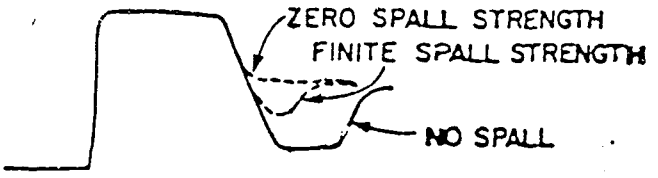

Fig.9 Expected manganin gauge signal from the back-surface configuration in the absence of spalling and as a function of the spall strength.

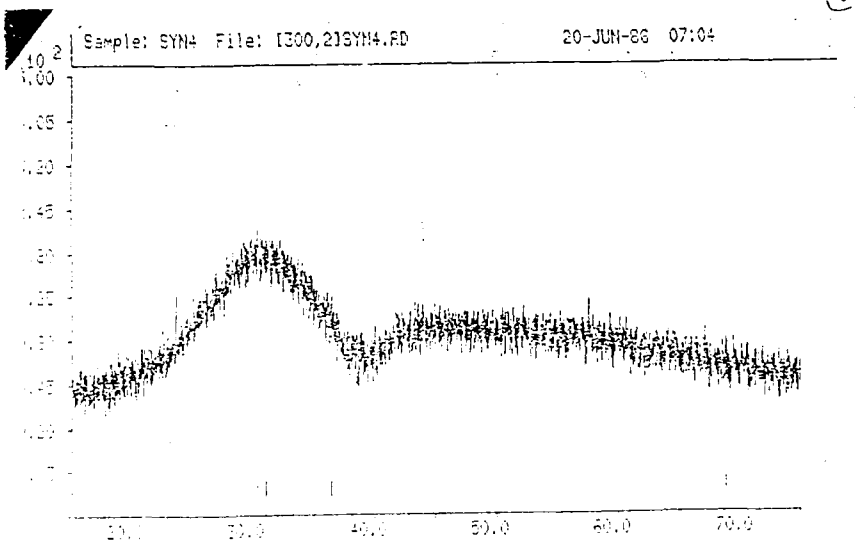

Fig.10 X-ray diffraction (XRD) spectrum from glass composition 'a' showing absence of crystalline phases.

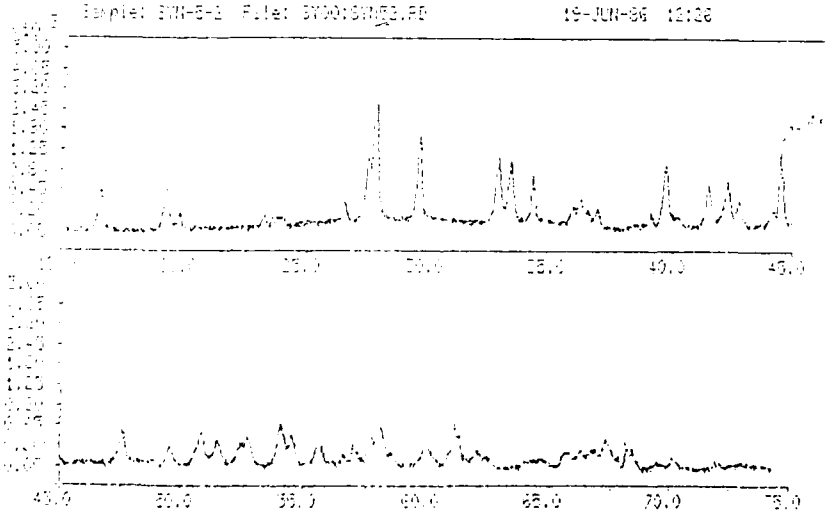

Fig.11 XRD spectrum from sample with 20 wt% TiB_2. Both TiB_2 and additional lines are observed.

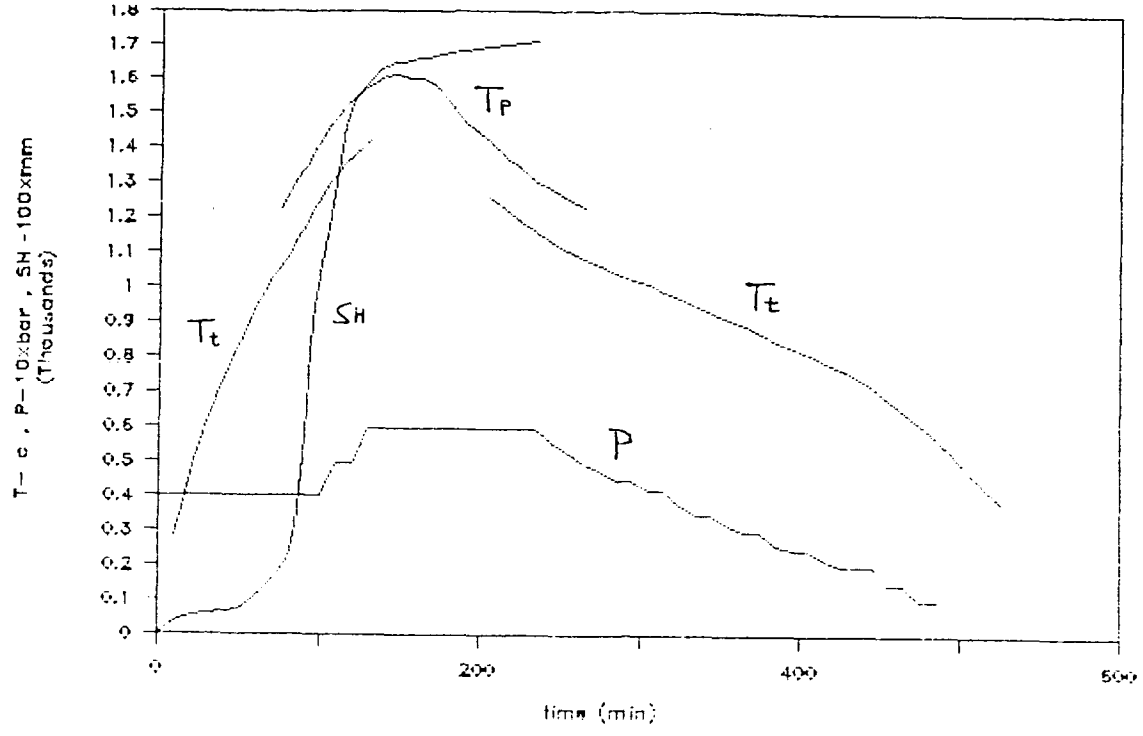

(a) Standard (fast) cycle used for 30mm diameter samples.

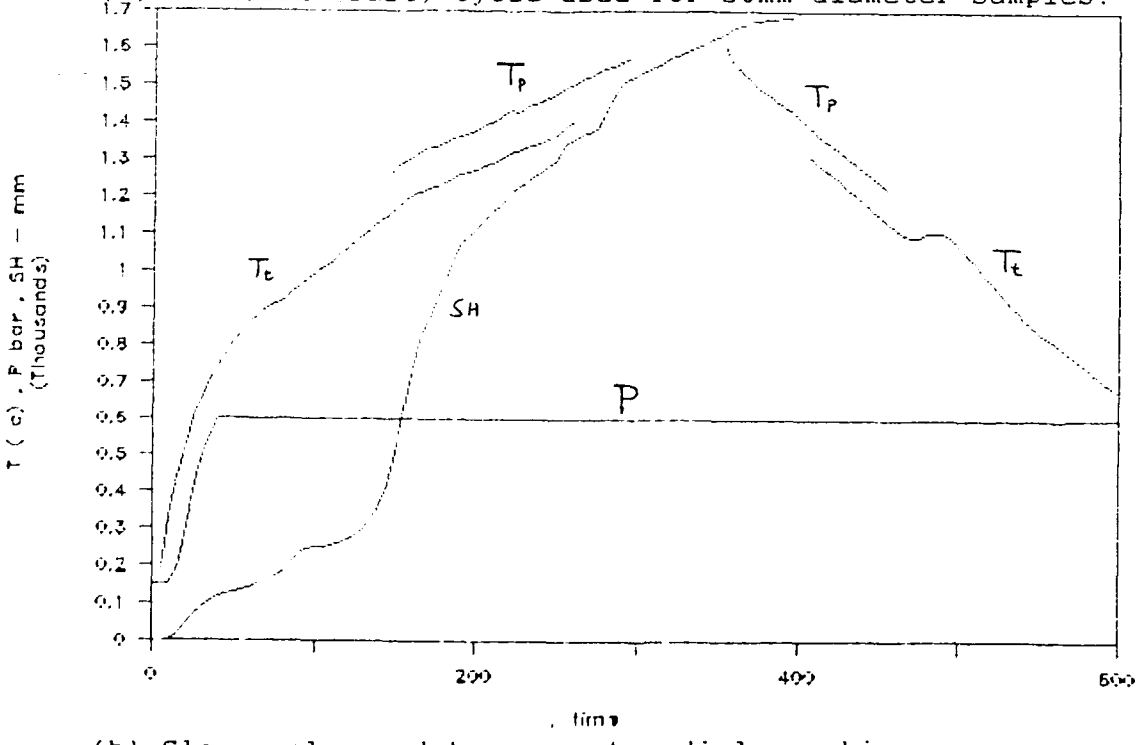

(b) Slow cycle used to prevent radial cracking.

Fig.12 Recorded hot-pressing cycles. T_t - thermocouple reading, T_p - pyrometer reading, P - applied pressure, Sh - observed piston displacement ('shrinkage').

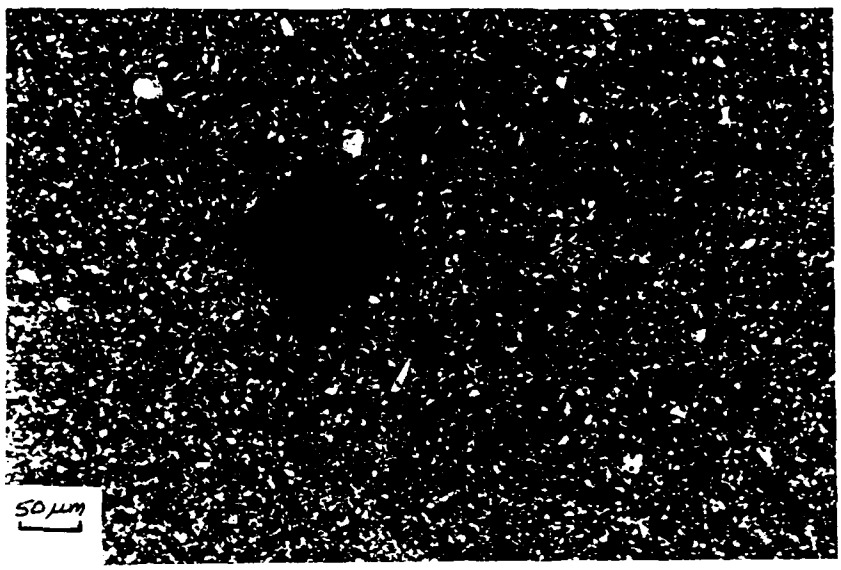

(a) Optical micrograph of specimen containing 15 wt% HSC077.

(b) TEM images (bright field, left; dark field, right) of specimen containing 50 wt% HSC059 grade.

Fig.13 Distribution of SiC particles.

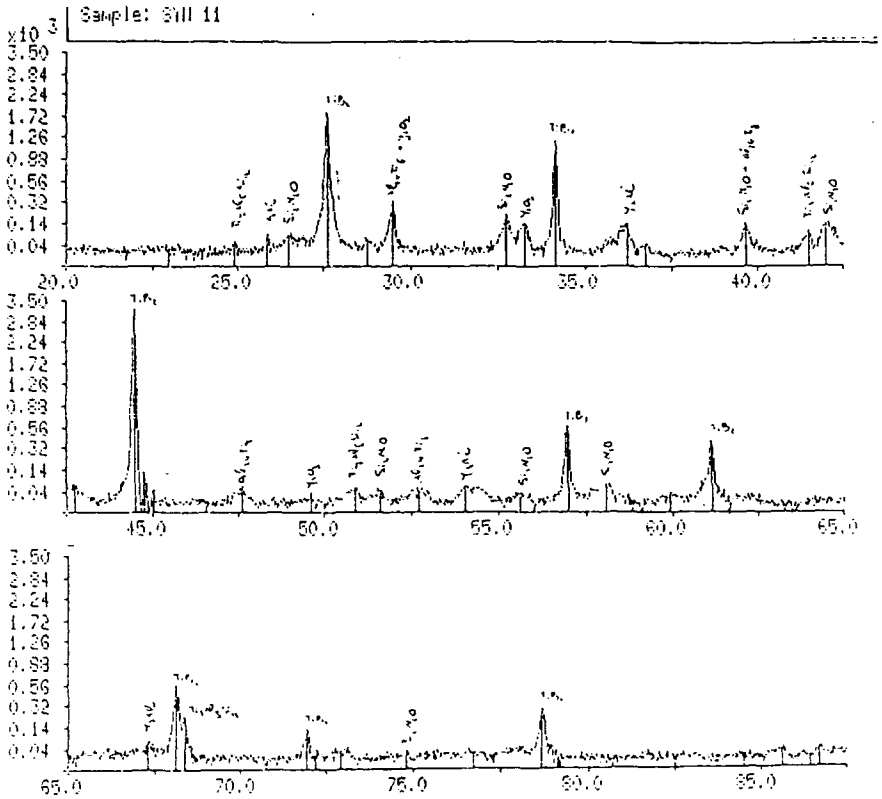

Fig.14 XRD spectrum from specimen containing 60 wt% TiB_2. The extra lines are associated with Ti-Al and Y-Al compounds, as well as Si_2ON_2.

(a) Si_2ON_2 particle: dark field image and selected area diffraction (SAD) pattern.

Fig.15 Transmission electron micrographs (TEM) of crystalline phases in TiB_2-containing specimens.

(b) $YAlO_3$ particle: dark field image and SAD pattern.

(c) $YAlO_3$ (left) and $Y_4Al_2O_9$ (right) particles: bright field and dark field micrographs.

Fig.15 (cont.) Transmission electron micrographs (TEM) of crystalline phases in TiB_2-containing specimens.

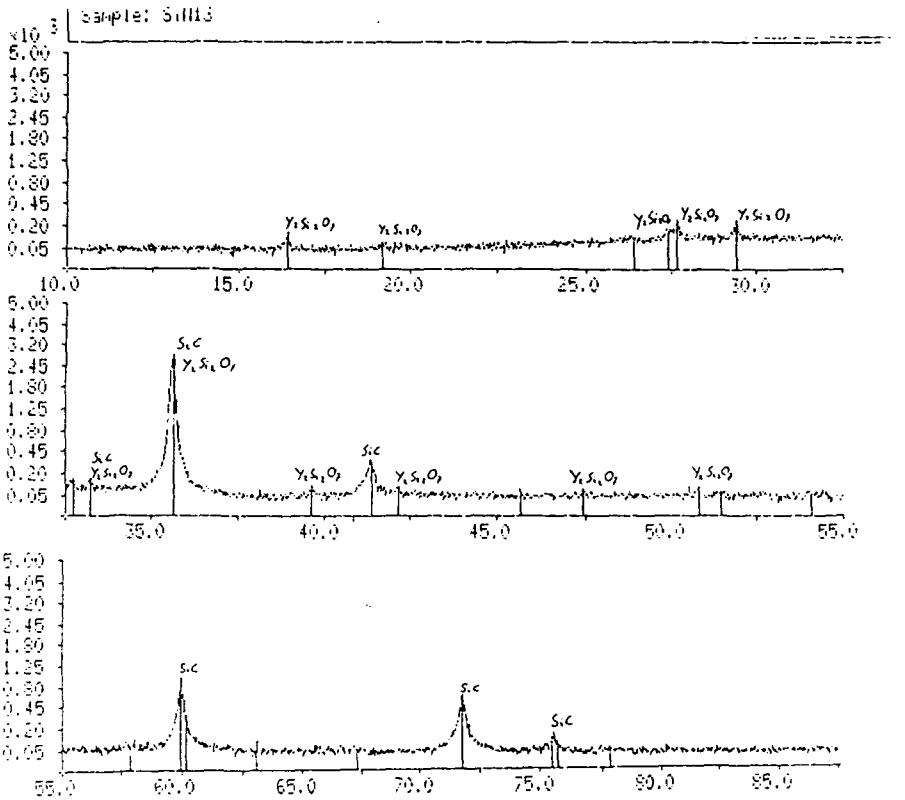

Fig.16 XRD spectrum of SiC-containing glass showing evidence of $Y_2Si_2O_7$ precipitation.

Fig.17 TEM bright field and dark field images of Al_2SiO_5 in specimen with SiC filler.

Fig.18 Fracture surface of specimen containing 15 wt% of coarse grained SiC filler powder.

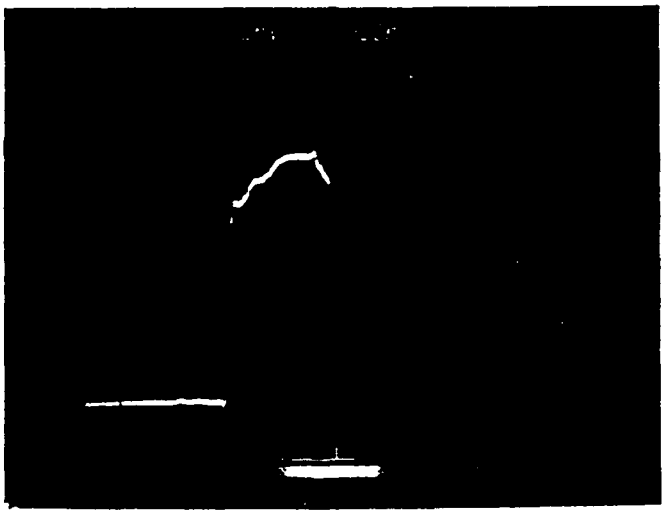

Fig.19 Pulse record from a 'back-surface' gauge impact test.

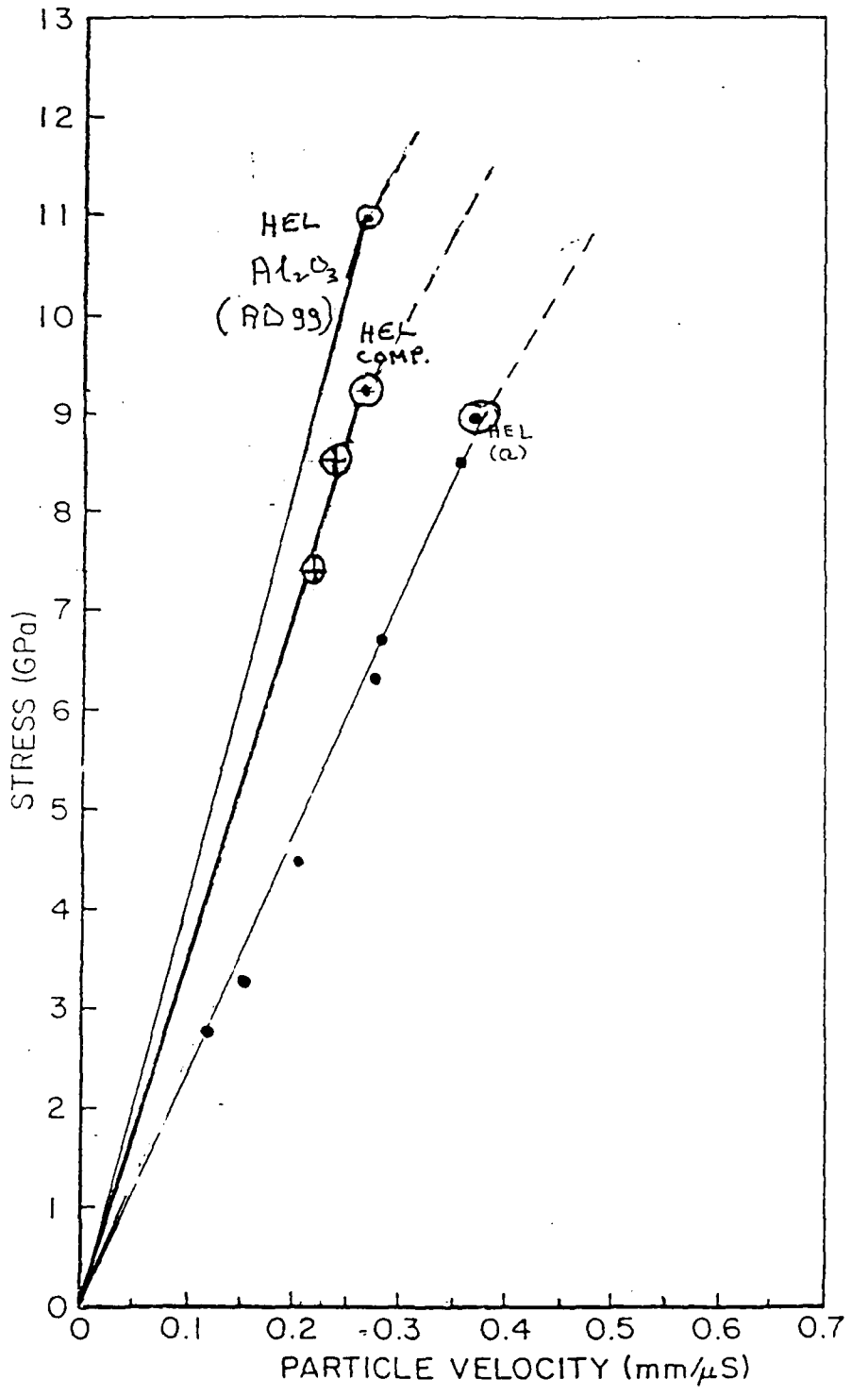

Fig.20 Hugoniot curve for the particulate composite compared with that of the oxynitride glass and that of 99.9% Al_2O_3.